LETTERS
PUBLISHED ONLINE: 6 JUNE 2016 | DOI: 10.1038/NCLIMATE3046
nature climate change

Potential evapotranspiration and continental drying

P. C. D. Milly* and K. A. Dunne

By various measures (drought area[1] and intensity[2], climatic aridity index[3], and climatic water deficits[4]), some observational analyses have suggested that much of the Earth's land has been drying during recent decades, but such drying seems inconsistent with observations of dryland greening and decreasing pan evaporation[5]. 'Offline' analyses of climate-model outputs from anthropogenic climate change (ACC) experiments portend continuation of putative drying through the twenty-first century[3,6–10], despite an expected increase in global land precipitation[9]. A ubiquitous increase in estimates of potential evapotranspiration (PET), driven by atmospheric warming[11], underlies the drying trends[4,8,9,12], but may be a methodological artefact[5]. Here we show that the PET estimator commonly used (the Penman–Monteith PET[13] for either an open-water surface[1,2,6,7,12] or a reference crop[3,4,8,9,11]) severely overpredicts the changes in non-water-stressed evapotranspiration computed in the climate models themselves in ACC experiments. This overprediction is partially due to neglect of stomatal conductance reductions commonly induced by increasing atmospheric CO_2 concentrations in climate models[5]. Our findings imply that historical and future tendencies towards continental drying, as characterized by offline-computed runoff, as well as other PET-dependent metrics, may be considerably weaker and less extensive than previously thought.

PET, simply put, is the rate at which evapotranspiration occurs when the surface is well supplied with water. In ACC impact studies conducted 'offline' (that is, outside climate models), the Penman–Monteith method has been used to transform climate-model outputs to PET, which, in turn, is an input to a variety of aridity indices, drought indices, and hydrologic impact models. Either one or the other of two variants of the Penman–Monteith equation frequently is used. The first (commonly called the Penman potential evaporation equation, and here referred to as PET-OW) assumes an open-water surface of specified roughness; the second (PET-RC) corresponds to an idealized reference crop of constant roughness and bulk stomatal conductance, fully shading the ground. In either case, Penman–Monteith PET is computed as an approximate linearized solution of a system of physics-based equations governing energy balance, thermodynamic state, and vertical heat and water-vapour diffusion. As such, Penman–Monteith PET is a relatively simple approximation to a nonlinear system of equations commonly solved in a climate model, in which heterogeneous vegetation and ground surface interact by radiative and diffusive transport.

Climate models do not compute PET, but rather compute actual evapotranspiration (ET). Nevertheless, we can test Penman–Monteith PET estimates for consistency with the climate models from which they are derived. This is because ET in the models is not water limited in some regions during some seasons of the year. Under such conditions, PET should, by definition, be equal to the actual ET computed in the climate model that supplies the data for PET computation. As a critical corollary, the sensitivities of (offline) PET and (climate-model) non-water-stressed ET (NWSET) to climate change should be equal. To the extent that these differ, they indicate that the offline impacts do not faithfully represent the climate-model physics.

Here, we compare changes in NWSET and PET (dNWSET and dPET) from the historical period 1981–2000 to the future period 2081–2100 in a suite of climate models under the Coupled Model Intercomparison Project Phase 5 (CMIP5) historical and Representative Concentration Pathway 8.5 (RCP8.5) experiments (Methods). We evaluate both PET-OW and PET-RC. Our data analysis uses only those climate-model grid-cells and months of the year where and when water stress is absent in both historical and future time periods (Methods; Supplementary Fig. 1). We also limit the data to those grid-cells/months for which the air temperature at reference level (2 m) is greater than 10 °C; this avoids dealing with frozen water and focuses the analysis on conditions under which ET is a major component of the water balance. We use the same 16 CMIP5 climate models that were used in an earlier analysis of PET[10] (Supplementary Table 1) and perform computations (except as noted) on a monthly time step, as is most commonly done in the literature.

The single-model mean NWSET (area-weighted, over all of the non-water-stressed grid-cells/months in a given model) during the historical period ranged from 3.1 to 4.5 (median 3.8) mm d^{-1} across models. The corresponding average of dNWSET varied across models from −0.03 to 0.38 (median 0.23) mm d^{-1} (Fig. 1). dNWSET varied spatially and temporally within each model; the fraction of non-water-stressed grid-cells/months where NWSET decreased from the historical to future time period ranges across models from 0.04 to 0.51 (median 0.16) mm d^{-1}.

Consistent with earlier findings[11], PET-RC (as well as PET-OW) predicts NWSET fairly well (Supplementary Fig. 2). Biases in single-model means of PET-RC range from −1.2 to 0.4 (median −0.5) mm d^{-1}. However, century-scale changes in means of both PET-OW and PET-RC generally far exceed the changes in mean NWSET in most of the climate models (Fig. 1). Single-model mean values of the difference between dPET-RC and dNWSET range from 0.03 to 0.52 (median 0.26) mm d^{-1} across models. Biases of dPET-OW are similar in magnitude. These dPET biases are of the same order of magnitude as dNWSET itself.

Why do the Penman–Monteith estimators of PET perform so poorly in this test? An important aspect of the ACC experiments is the increase in atmospheric CO_2 concentration, by more than a factor of two, during the RCP8.5 scenario. We reasoned that neglect of the resultant climate-model changes in bulk stomatal conductance[5] could explain much of the failure of both variants of the Penman–Monteith dPET to predict dNWSET. To test

US Geological Survey and NOAA/Geophysical Fluid Dynamics Laboratory, Princeton, New Jersey 08540, USA. *e-mail: cmilly@usgs.gov

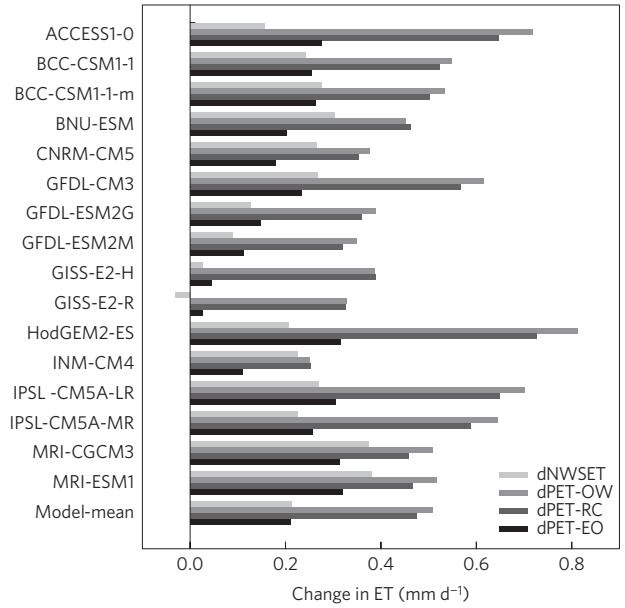

Figure 1 | Changes (future — historical; mm d^{-1}) of ET. Bars represent area-weighted averages over all non-water-stressed grid-cells/months, of climate-model non-water-stressed ET (dNWSET), reference-crop Penman–Monteith PET (dPET-RC), open-water Penman–Monteith PET (dPET-OW) and energy-only PET (dPET-EO) for each of 16 CMIP5 climate models and for the multi-model mean.

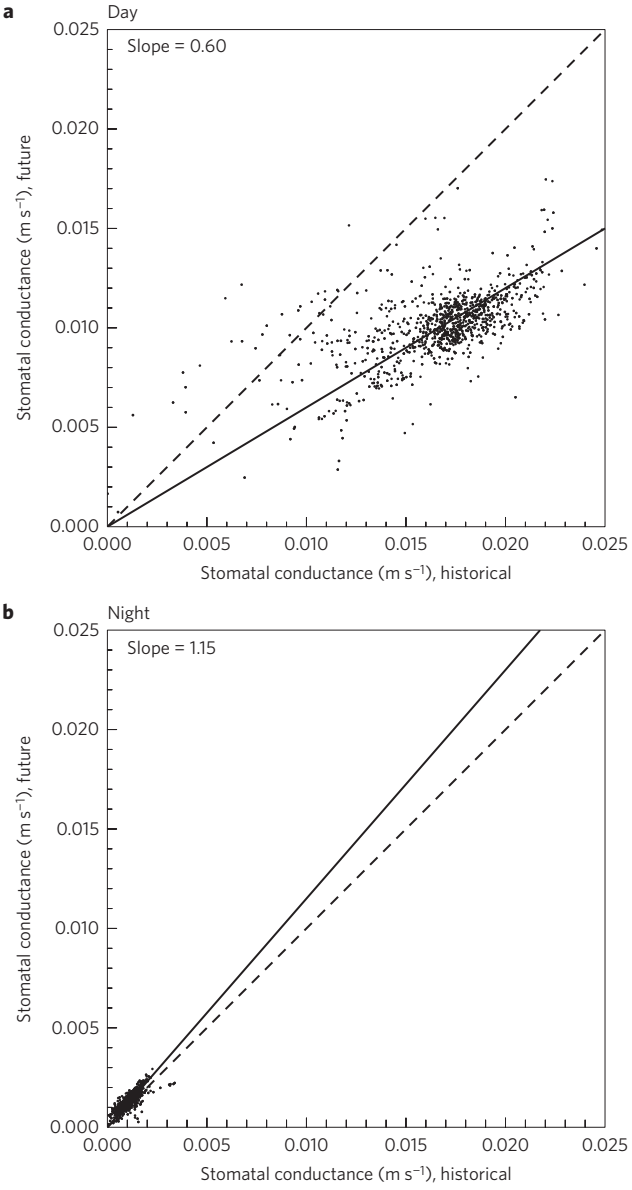

Figure 2 | Future versus historical stomatal conductance (m s^{-1}), for the GFDL-ESM2M climate model. a,**b** Plots are for daytime (**a**) and night-time (**b**). Each point represents a time average for one non-water-stressed grid-cell/month. Dashed lines are slope-1 lines through the origin, and solid lines are least-squares fits through the origin.

this idea, we first re-ran the GFDL-ESM2M model to obtain output of bulk stomatal conductance; stomatal conductance outputs are not generally available for CMIP5. We found that daytime values of non-water-stressed bulk stomatal conductance were typically 40% smaller during the future period than during the historical period (Fig. 2); night-time values showed little systematic change from historical to future. We then recomputed dPET-RC with output from the GFDL-ESM2M model, but (because most evapotranspiration occurs during the daytime) with a 40% smaller bulk stomatal conductance (Methods) for the future time period (dPET-RC.6); we also recomputed the usual dPET-RC, as well as dPET-OW. The open-water and reference-crop Penman–Monteith methods yielded dNWSET prediction biases (Fig. 3) of 0.24 and 0.21 mm d^{-1} for GFDL-ESM2M. With its 40% future reduction in stomatal conductance, however, dPET-RC.6 showed a reduced, but substantial, bias of 0.09 mm d^{-1} in prediction of dNWSET.

Evidently, neglect of changing stomatal conductance is the largest contributor to dPET bias, but is not the only significant discrepancy between climate-model computation of dNWSET and standard (that is, constant-conductance) computations of Penman–Monteith dPET. In a climate model, absorption of radiation, and consequent vaporization of water, generally occur both at the ground surface and in the canopy, through a resistance network more complex than that in the Penman–Monteith theory. Climate-model surface fluxes are parameterized in terms of the gradient of thermodynamic state between the surface and the lowest atmospheric model level, which usually is considerably greater than 2 m above ground; this, in turn, means that sensible heat fluxes are parameterized in terms of the gradient of potential temperature, rather than temperature. Climate models consider the effect of intercepted water on vegetation. Climate-model computations are performed on a short (for example, 30-min) time step rather than monthly. To correct for all of these discrepancies, we adopted the Shuttleworth–Wallace[14] two-source (vegetation and ground) model of ET and adapted it to include effects of potential temperature and interception, with computations performed on the climate-model time step. Use of this extended Shuttleworth–Wallace estimator (dPET-SW) reduced the bias in prediction of dNWSET to 0.07 mm d^{-1} (Fig. 3). We conclude that standard application of Penman–Monteith PET to computing multi-decadal dNWSET fails largely because of neglect of changing stomatal conductance, but also because of a combination of various factors that can be captured only by detailed analysis and that undoubtedly differ from one climate model to the next.

In view of the complexity needed to reproduce (approximately) climate-model processes in offline computations, can we find an alternative approach to estimation of PET for impact studies of continental drying and of water resources in general? Here we modify and evaluate a very simple estimator of PET that is based on the idea that long-term latent heat flux of PET is equal to the net radiation absorbed at the land surface[15,16]. We generalize this to apply (when ground heat flux also is accounted for) on a monthly timescale; and to specify that a fixed fraction (and not necessarily all) of available

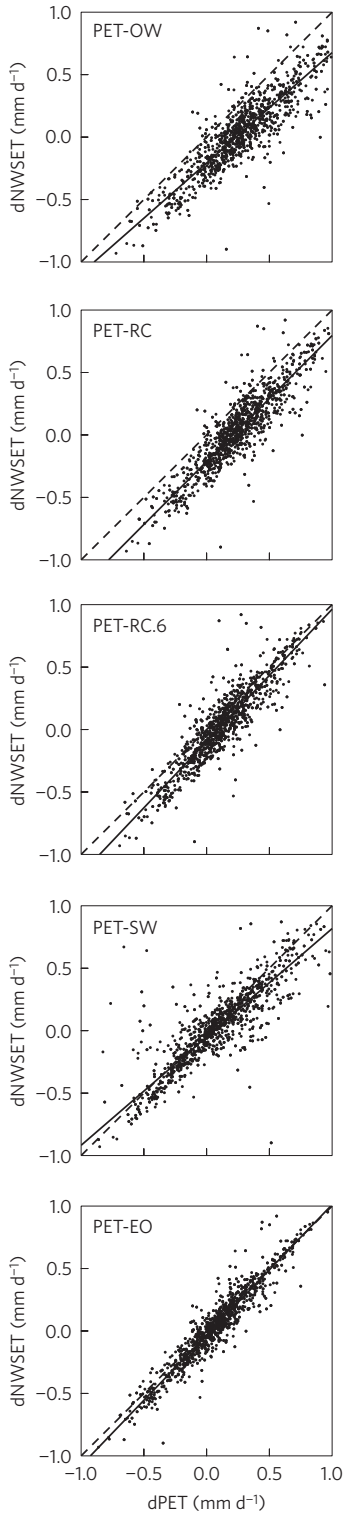

Figure 3 | Scatter plot of change in non-water-stressed ET from the GFDL-ESM2M climate model (dNWSET) against change in PET (dPET). dPET is computed by (top to bottom) the open-water Penman–Monteith method (PET-OW), the reference-crop Penman–Monteith method (PET-RC), the reference-crop Penman–Monteith method modified to have stomatal conductance reduced to 60% of the standard value during the future period (PET-RC.6), the Shuttleworth–Wallace method (PET-SW) and the energy-only method (PET-EO). Each point represents a difference between historical and future 20-year averages for one non-water-stressed grid-cell/month. Dashed lines are slope-1 lines through the origin, and solid lines are Theil–Sen estimators.

energy goes into latent heat flux of NWSET. An observation-model analysis[17] that implicitly assumed such a relation determined this fraction to be about 80%, indicating that not all available energy goes into ET, even under non-water-stressed conditions. We call this energy-based PET estimator the energy-only PET (PET-EO), following terminology introduced[11] for the special case where the fraction is 100%, but we use the 80% fraction here.

Single-climate-model biases of dPET-EO averaged over all non-water-stressed grid-cells/months are much smaller than for the Penman–Monteith methods (Fig. 1), ranging from −0.12 to 0.12 (median 0.02) mm d^{-1} across models. The simple dPET-EO estimates for individual grid-cells/months in GFDL-ESM2M (Fig. 3) are more accurate (bias 0.03 mm d^{-1}) than those for the complex dPET-SW estimates (bias 0.07 mm d^{-1}).

Our test of PET estimators is directly meaningful only for non-water-stressed conditions; fortunately, these are precisely the conditions under which water balance is most sensitive to PET. (When conditions are drier, evapotranspiration is limited more by water availability than by energy availability, which is quantified by PET.) But how can we evaluate PET and its effect on water balance for the full range of water-stress status? Annual mean PET and precipitation can be used to estimate annual mean ET and runoff through Budyko's water-balance relation[15,16] (Methods). Using this relation, we computed historical and future runoff from climate-model precipitation combined with each PET estimator: PET-OW, PET-RC and PET-EO. The changes in runoff so computed were compared with changes of long-term means of runoff directly from the climate models. Both of the Penman–Monteith PET estimators led to excessive increases in evapotranspiration, which, in turn, caused (Fig. 4) excessive decreases of runoff in regions where the climate models projected decreased runoff (for example, northern South America, southern Africa, southeastern Australia), as well as some decreases in runoff even where the climate models showed increased runoff (for example, central Africa). In contrast, the energy-only PET estimator captured much better, although not perfectly, the magnitudes and global pattern of runoff changes from the climate model. Global land average of relative change in runoff from the climate models was +6%; for PET-OW and PET-RC it was −4% and −5%, and for PET-EO it was +6%.

The simplicity of the energy-only PET method contrasts sharply with the impractical complexity needed to achieve similar accuracy with an offline formulation based on surface meteorological variables. Surface variables are tightly coupled through feedbacks that, possibly, cause them approximately to obey the simple, top-down energy constraint embodied in the energy-only method; bottom-up efforts to estimate each of the variables and all of their interactions is difficult and, perhaps, unnecessary. In fact, when we repeated the GFDL-ESM2M computations for Fig. 1, but instead used historical and future experiments in which stomata cannot 'see' the changes in atmospheric CO_2 concentration, we still found that the dPET-EO estimator outperformed dPET-OW and dPET-RC. Thus, factors other than neglect of CO_2-induced stomatal closure seem to contribute to failure of the Penman–Monteith methods, as often implemented. Such factors could include climate-induced changes of stomatal conductance and (stability-dependent) surface aerodynamic resistance.

Global climate models, despite their coarse spatial resolution and imperfect physical parameterizations, are nevertheless internally consistent representations of the climate system. Care must be taken in the use of external impact models for the analysis and/or refinement (for example, spatial downscaling) of the output of climate models, lest inconsistencies be introduced that seriously degrade, rather than enhance, their information content. This is particularly true for the use of PET, a hypothetical construct that generally is neither anchored by direct measurement nor computed in climate models, but is nevertheless often used in several measures

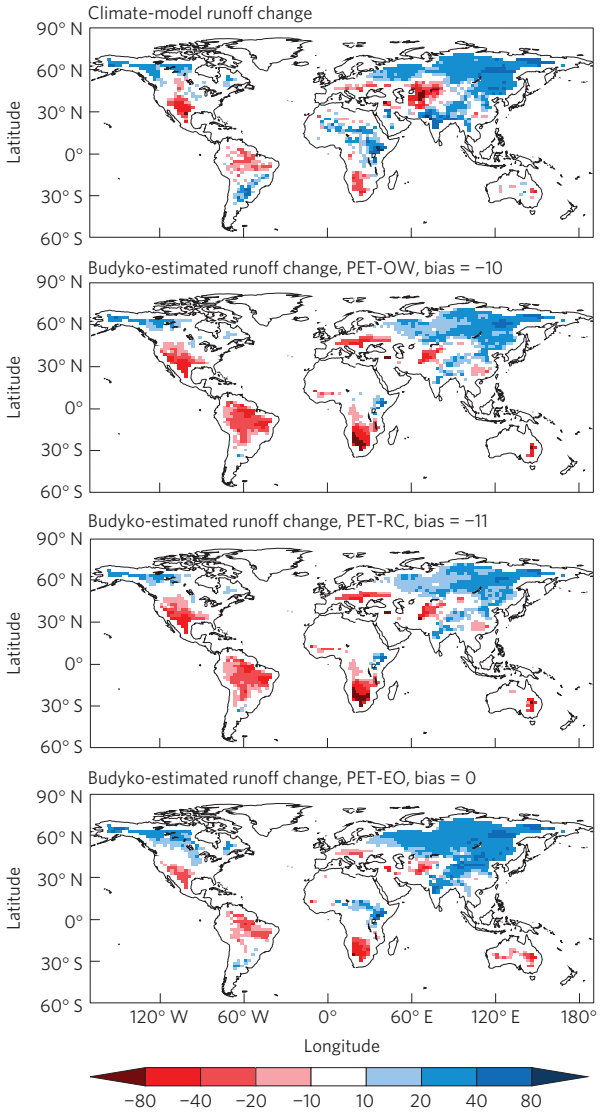

Figure 4 | Multi-model median of the relative change (%) of the annual-mean runoff from the historical to the future time period. Maps show results (top to bottom) from climate-model output; from the Budyko water-balance model (Methods) in conjunction with estimated PET-OW and climate-model output of precipitation; from the Budyko water-balance model in conjunction with estimated PET-RC and climate-model output of precipitation; and from the Budyko water-balance model in conjunction with estimated PET-EO and climate-model output of precipitation. The 'bias' is the mean error relative to climate-model runoff change. Relative change computed as (future − historical)/[(future + historical)/2]. Greenland is excluded from the analysis.

of impact. Such measures include offline-computed runoff[18] and soil moisture[19], climatic aridity index[3] (ratio of precipitation to PET), and Palmer Drought Severity Index[1,2,6,8]. Our findings suggest that PET-change biases could lead to overestimation of ACC drying trends in such variables. Drying trends might more meaningfully be assessed by direct examination of climate-model variables (for example, runoff[20], actual ET, soil moisture[21], and relative humidity[22]) themselves and/or by use of the energy-only PET estimator in offline impact studies, if further studies support its robustness.

Methods

Methods and any associated references are available in the online version of the paper.

Received 30 September 2015; accepted 3 May 2016; published online 6 June 2016

References

1. Dai, A. Characteristics and trends in various forms of the Palmer Drought Severity Index during 1900–2008. *J. Geophys. Res.* **116,** D12115 (2011).
2. Sheffield, J., Wood, E. F. & Roderick, M. L. Little change in global drought over the past 60 years. *Nature* **491,** 435–438 (2012).
3. Feng, S. & Fu, Q. Expansion of drylands under a warming climate. *Atmos. Chem. Phys.* **13,** 10081–10094 (2013).
4. McCabe, G. J. & Wolock, D. M. Increasing Northern Hemisphere water deficit. *Climatic Change* **132,** 237–249 (2015).
5. Roderick, M. L., Greve, P. & Farquhar, G. D. On the assessment of aridity with changes in atmospheric CO_2. *Wat. Resour. Res.* **51,** 5450–5463 (2015).
6. Burke, E. J., Brown, S. J. & Christidis, N. Modeling the evolution of global drought and projections for the twenty-first century with the Hadley Centre climate model. *J. Hydrometeorol.* **7,** 1113–1125 (2006).
7. Dai, A. Increasing drought under global warming in observations and models. *Nature Clim. Change* **3,** 52–58 (2012).
8. Cook, B. I., Smerdon, J. E., Seager, R. & Coats, S. Global warming and 21st century drying. *Clim. Dyn.* **43,** 2607–2627 (2014).
9. Fu, Q. & Feng, S. Responses of terrestrial aridity to global warming. *J. Geophys. Res. Atmos.* **119,** 7863–7875 (2014).
10. Scheff, J. & Frierson, D. M. W. Terrestrial aridity and its response to greenhouse warming across CMIP5 climate models. *J. Clim.* **28,** 5583–5600 (2015).
11. Scheff, J. & Frierson, D. M. W. Scaling potential evapotranspiration with greenhouse warming. *J. Clim.* **27,** 1539–1558 (2014).
12. Dai, A. Drought under global warming: a review. *WIREs Clim. Change* **2,** 45–65 (2011).
13. Shuttleworth, W. J. *Handbook of Hydrology* (ed. Maidment, D. R.) Ch. 4 (McGraw-Hill, 1993).
14. Shuttleworth, W. J. & Wallace, J. S. Evaporation from sparse crops—an energy combination theory. *Q. J. R. Meteorol. Soc.* **111,** 839–855 (1985).
15. Budyko, M. I. *Climate and Life* (Academic, 1974).
16. Roderick, M. L., Sun, F., Lim, W. H. & Farquhar, G. D. A general framework for understanding the response of the water cycle to global warming over land and ocean. *Hydrol. Earth Syst. Sci.* **18,** 1575–1589 (2014).
17. Koster, R. D. & Mahanama, S. P. P. Land surface controls on hydroclimatic means and variability. *J. Hydrometeorol.* **13,** 1604–1620 (2012).
18. Schewe, J. *et al*. Multimodel assessment of water scarcity under climate change. *Proc. Natl Acad. Sci. USA* **111,** 3245–3250 (2014).
19. Chiew, F. H. S., Whetton, P. H., McMahon, T. A. & Pittock, A. B. Simulation of the impacts of climate change on runoff and soil moisture in Australian catchments. *J. Hydrol.* **167,** 121–147 (1995).
20. Milly, P. C. D., Dunne, K. A. & Vecchia, A. V. Global pattern of trends in streamflow and water availability in a changing climate. *Nature* **438,** 347–350 (2005).
21. Cook, B. I., Ault, T. R. & Smerdon, J. E. Unprecedented 21st century drought risk in the American Southwest and Central Plains. *Sci. Adv.* **1,** e1400082 (2015).
22. Sherwood, S. & Fu, Q. A drier future? *Science* **343,** 737–739 (2014).

Acknowledgements

The World Climate Research Programme's Working Group on Coupled Modelling is responsible for CMIP; the climate modelling groups listed in Supplementary Table 1 produced, and made available, their model output. For CMIP, the US Department of Energy's Program for Climate Model Diagnosis and Intercomparison provides coordinating support and led development of software infrastructure in partnership with the Global Organization for Earth System Science Portals. A. Berg, S. Kapnick, M. Roderick, J. Scheff and G. Wang gave helpful reviews of our manuscript.

Author contributions

P.C.D.M. conceived and led the study, interpreted the data and prepared the manuscript. K.A.D. carried out all computations, prepared all figures and assisted with manuscript preparation.

Additional information

Supplementary information is available in the online version of the paper. Reprints and permissions information is available online at www.nature.com/reprints. Correspondence and requests for materials should be addressed to P.C.D.M.

Competing financial interests

The authors declare no competing financial interests.

Methods

Climate-model data. We employed output from 16 climate models participating in Phase 5 of the Coupled Model Intercomparison Project (CMIP5; Supplementary Table 1). We used monthly-average model outputs of precipitation, evaporation, and runoff; surface pressure and sensible and latent heat fluxes; and near-surface wind speed, specific humidity, and temperature. For the ACCESS1-0 and HadGEM2-ES models, runoff output was not available and so was estimated as the difference between precipitation and evapotranspiration. For the GFDL-ESM2M model, we also used half-hourly (that is, climate-model time-step) output of the aforementioned variables, as well as bulk stomatal resistance and several other variables needed for the Shuttleworth–Wallace equations (presented below). We used 1981–2000 data for the historical experiment and 2081–2100 data for the RCP8.5 ('future') experiment.

Selection of data. We used data for grid-cells/months where non-water-stressed conditions were present in both historical and future periods; monthly ratio of ET to precipitation was less than 2; and reference-level temperature was greater than 10 °C. We evaluated these conditions separately for each climate model on its own grid and then interpolated results to a common grid. To determine locations and times of year when evapotranspiration was non-water-stressed, we examined the sensitivity of monthly evapotranspiration to same-month precipitation. For each model, for the historical and future experiment separately, for each month of the year and for each grid-cell, we fitted a parabola of evapotranspiration against precipitation; each fit used 20 data points, representing the 20 years of data. For each value of precipitation, we evaluated the slope of the parabola and then found the maximum of those 20 slopes. We defined as non-water-stressed those locations and months of the year where, for both the historical and the future periods, the maximum slope was less than 0.05 and the ratio of actual evapotranspiration to precipitation was less than 2. The latter condition eliminated data where slope estimates were unstable owing to sensitivity of evapotranspiration to precipitation stored from earlier months. A sensitivity test using a maximum slope of 0.1 yielded a larger data set, with qualitatively similar results to those found for 0.05, but also produced more outlier points in Fig. 3. In many non-water-stressed regions/seasons, the sensitivity of evapotranspiration to precipitation was actually negative, reflecting the negative correlation between radiation and precipitation[23]. Supplementary Fig. 1 maps the multi-model mean of the number of months of data chosen for analysis.

Open-water Penman–Monteith PET. Open-water Penman–Monteith PET (mm d^{-1} (equivalent to kg m^{-2} d^{-1})) (often called Penman potential evaporation) was calculated as[13]

$$\mathrm{PET}=\frac{\Delta}{\Delta+\gamma}(R_\mathrm{n}-G)+\frac{\gamma}{\Delta+\gamma}\frac{6.43(1+0.536u)(e_\mathrm{s}-e_\mathrm{a})}{L_\mathrm{v}} \quad (1)$$

in which R_n (mm d^{-1}) and G (mm d^{-1}) are net radiation at the surface and heat flux into the subsurface, expressed in equivalent ET units; e (kPa) and u (m s^{-1}) are, respectively the vapour pressure and wind speed, both at 2 m height; $L_\mathrm{v}(T)$ is latent heat of vaporization of water (MJ kg^{-1}), given by

$$L_\mathrm{v}(T)=2.501-0.002361T \quad (2)$$

in which T (°C) is air temperature at 2 m height; e_s (kPa) and Δ (kPa K^{-1}) are the saturation vapour-pressure function and its derivative with respect to T, evaluated at temperature T; and γ (kPa K^{-1}) is the psychrometric constant. (Equation (2) is also used in the conversion of $R_\mathrm{n}-G$ in (1) to units of ET.) The quantities e_s, Δ and γ are computed according to

$$e_\mathrm{s}=0.6108\exp[17.27T/(T+237.3)] \quad (3)$$

$$\Delta=4098e_\mathrm{s}/(T+237.3)^2 \quad (4)$$

$$\gamma=0.0016286P/L_\mathrm{v} \quad (5)$$

in which P (kPa) is atmospheric pressure at the surface.

Reference-crop Penman–Monteith PET. Reference-crop Penman–Monteith PET (mm d^{-1}) was calculated as[24]

$$\mathrm{PET}=\frac{0.408\Delta(R_\mathrm{n}-G)+\gamma\dfrac{900}{T+273}u(e_\mathrm{s}-e)}{\Delta+\gamma(1+0.34u)} \quad (6)$$

in which $R_\mathrm{n}-G$ is expressed in MJ m^{-2} d^{-1} and

$$\gamma=0.000665P \quad (7)$$

The constants 900 and 0.34 are for daily (or longer timescale) computations for a short reference crop of height 0.12 m and a fixed surface resistance of 70 s m^{-1}. Here we follow the practice of most investigators, using a monthly time step. (In one study[11], computations were performed on a 3-hourly time step, but a subsequent study[10] showed relative insensitivity of computed PET change to computational time step.) The 0.34 constant is inversely proportional to stomatal conductance[24], so we divide it by 60% to implement the RC.6 computation for GFDL-ESM2M.

Energy-only PET. We compute the energy-only PET by

$$\mathrm{PET}=0.8(R_\mathrm{n}-G) \quad (8)$$

with all variables expressed in mm d^{-1}, again using equation (2).

Shuttleworth–Wallace PET. Shuttleworth and Wallace[14] derived a solution for evapotranspiration from 'sparse crops' (that is, situations where both the vegetation and the ground may contribute substantially to ET). Their conceptual model for the surface is similar to that used in many climate models. The flux of heat and water vapour from the surface to the canopy-air space experiences an aerodynamic resistance to diffusion given by r_a^s; aerodynamic resistances from canopy-air space to reference level in the atmosphere and from canopy-air space to plant are given by r_a^a and r_a^c respectively. Additional resistances to vapour transport are a bulk stomatal resistance r_s^c between plant tissue and plant exterior and a surface resistance r_s^s, expressing water limitation at the soil surface. The solution for ET is

$$L_\mathrm{v}\mathrm{ET}=C_\mathrm{c}\mathrm{PM}_\mathrm{c}+C_\mathrm{s}\mathrm{PM}_\mathrm{s} \quad (9)$$

$$\mathrm{PM}_\mathrm{c}=\frac{\Delta A+\{\rho c_p(e_\mathrm{s}-e)-\Delta r_\mathrm{a}^\mathrm{c}A_\mathrm{s}\}/(r_\mathrm{a}^a+r_\mathrm{a}^\mathrm{c})}{\Delta+\gamma\{1+r_\mathrm{s}^\mathrm{c}/(r_\mathrm{a}^a+r_\mathrm{a}^\mathrm{c})\}} \quad (10)$$

$$\mathrm{PM}_\mathrm{s}=\frac{\Delta A+\{\rho c_p(e_\mathrm{s}-e)-\Delta r_\mathrm{a}^\mathrm{s}(A-A_\mathrm{s})\}/(r_\mathrm{a}^a+r_\mathrm{a}^\mathrm{s})}{\Delta+\gamma\{1+r_\mathrm{s}^\mathrm{s}/(r_\mathrm{a}^a+r_\mathrm{a}^\mathrm{s})\}} \quad (11)$$

$$C_\mathrm{c}=\{1+R_\mathrm{c}R_\mathrm{a}/R_\mathrm{s}(R_\mathrm{c}+R_\mathrm{a})\}^{-1} \quad (12)$$

$$C_\mathrm{s}=\{1+R_\mathrm{s}R_\mathrm{a}/R_\mathrm{c}(R_\mathrm{s}+R_\mathrm{a})\}^{-1} \quad (13)$$

$$R_\mathrm{a}=(\Delta+\gamma)r_\mathrm{a}^a \quad (14)$$

$$R_\mathrm{s}=(\Delta+\gamma)r_\mathrm{a}^\mathrm{s}+\gamma r_\mathrm{s}^\mathrm{s} \quad (15)$$

$$R_\mathrm{c}=(\Delta+\gamma)r_\mathrm{a}^\mathrm{c}+\gamma r_\mathrm{s}^\mathrm{c} \quad (16)$$

In (10) and (11), $R_\mathrm{n}-G$ (now in W m^{-2}) is represented by A, and $A-A_\mathrm{s}$ is the portion of net radiation absorbed by the plant canopy. To make this model consistent with the GFDL-ESM2M model, we replaced r_s^c by an effective value, $r_\mathrm{s}^{\mathrm{c}*}$, to account for a doubled aerodynamic resistance to vapour transport, based on the idea that only one side of the leaf produces evapotranspiration; and partial coverage of a time-varying fraction $1-f$ of the active side of the leaf by intercepted water. The expression for $r_\mathrm{s}^{\mathrm{c}*}$ is the solution of

$$\frac{1}{r_\mathrm{s}^{\mathrm{c}*}+r_\mathrm{a}^\mathrm{c}}=\frac{(1-f)}{2r_\mathrm{a}^\mathrm{c}}+\frac{f}{r_\mathrm{s}^\mathrm{c}+2r_\mathrm{a}^\mathrm{c}} \quad (17)$$

To generalize the Shuttleworth–Wallace model for potential temperature, it can be shown that it is necessary only to evaluate e_s and Δ at the air temperature adjusted adiabatically to surface pressure.

The Shuttleworth–Wallace equations give actual ET. To obtain a Shuttleworth–Wallace PET, we express the absence of water stress by taking r_s^s equal to zero and r_s^c equal to its non-water-stressed value.

Computational details. Open-water, reference-crop and energy-only PET computations were performed on a monthly time step. Monthly values of surface radiation fluxes were available in the CMIP5 database for computation of R_n. However, because the CMIP5 database did not have data for G, we evaluated $R_\mathrm{n}-G$ by energy balance as $L_\mathrm{v}E+H$, where $L_\mathrm{v}E$ and H are latent and sensible heat fluxes at the surface, available as monthly averages from the CMIP5 database. Monthly values of T, q, P, and 10-m wind speed (U) also were available. Monthly values of specific humidity (q) were converted to e according to

$$e=Pq/(0.622+0.378q) \quad (18)$$

Values of U were converted to 2-m wind speeds by use of[24]

$$u = 0.75U \tag{19}$$

The Shuttleworth–Wallace PET computations were performed on a 30-min (that is, climate-model time-step) basis. The GFDL-ESM2M climate model was re-run for the periods 1981–2000 and 2081–2100 to produce output of the variables required for computations. To be entirely consistent with the climate-model formulation, we used the atmospheric state from the lowest atmospheric model layer instead of the 2-m and 10-m values. Latent heat flux was not output, so we computed it from evapotranspiration using (2). Half-hourly PET values were averaged to monthly values for evaluation.

Budyko water-balance relation. Historical and future climate-model precipitation, p, and estimated PET were converted to historical and future runoff, Y, by use of the simple Budyko water-balance model[15],

$$Y/p = 1 - \left[\frac{\mathrm{PET}}{p}\tanh\frac{p}{\mathrm{PET}}\left(1-\cosh\frac{\mathrm{PET}}{p}+\sinh\frac{\mathrm{PET}}{p}\right)\right]^{1/2} \tag{20}$$

In this equation, the variables are understood to represent 20-year mean values over the historical or future time periods.

References

23. Milly, P. C. D. & Dunne, K. A. Macroscale water fluxes 2. Water and energy supply control of their interannual variability. *Wat. Resour. Res.* **38,** 24-1–24-9 (2002).
24. Allen, R. G., Periera, L. S., Raes, D. & Smith, M. *Crop Evapotranspiration—Guidelines for Computing Crop Water Requirements* Irrigation and Drainage Paper 56, 15 (Food and Agricultural Organization of the United Nations, 1998).